Peer-Reviewed Technical Communication

Response of GPS-Tracked Drifters to Wind and Water Currents in a Tidal Estuary

Kabir A. Suara, Hang Wang, Hubert Chanson, Badin Gibbes, and Richard J. Brown

***Abstract*—Lagrangian field data in tidal shallow waters are rare, but valuable for the understanding of the spatiotemporal structure of flow and particle transport. The response of drifters to the wind and water flow in tidal shallow water was examined using correlation, spectral, and coherence analyses. Under moderate wind conditions (0–4 m/s), floating drifter motions in bounded sheltered water are affected by wind through low-frequency induced wind current rather than direct wind drag, when only a small portion of the drifter is unsubmerged. The field validation of both high- and low-resolution drifters with surface measured velocity from a fixed acoustic Doppler current profiler is good in the streamwise direction. The correlation between the drifter and fixed instrument velocities is low in the cross-stream direction due to strong spatial variability of the flow field. The evaluation shows that drifters are applicable to studying the flow dynamics of tidal water bodies in relation to small-scale processes.**

***Index Terms*—Coherence analysis, Eulerian instruments, Lagrangian drifters, shallow water, tidal estuary, validation.**

I. Introduction

LAGRANGIAN field data in tidal shallow waters are rare, but valuable for the understanding of the spatiotemporal structure flow and water qualities, validation of numerical models, and development of advection-dispersion models for such systems. There are many apparent difficulties associated with use of Global Positioning System (GPS)-tracked drifters in shallow tidal water, yet they can provide a rich source of information on the flow dynamics, level of mixing, and bathymetric influences on flow. Flow structures in small tidal estuaries have mainly been studied from the Eulerian perspective using acoustic devices sampled at high frequencies [1]. While a complete Eulerian approach using fixed acoustic devices gives limited insight to the spatial variability of the flow structures, a combined Eulerian–Lagrangian approach provides more complete evidence. For example, a Lagrangian drifter can provide velocity data at the shallow water surface where acoustic Doppler current profiler (ADCP) data are not suitable [2]. In addition, clusters of Lagrangian particle have be proven suitable for dispersion estimates traditionally carried out using more expensive dye tracer studies [3], [4]. Lagrangian studies using satellite-tracked drifters in estuaries that are limited to reasonably large tidal systems and inlets [5]–[7] and recently, a small tidal system [4].

Significant work has been done in terms of validating drifter motions in surf zones [8], [9] and recently in a tidal inlet [7]. In absence of "true" Lagrangian measurements, these validations are difficult because they were done when drifters are within close proximity to fixed Eulerian devices. The correlation of drifter motions with Eulerian devices varies with the instrument design and environment factors (e.g.,, water depth, boundaries, forcing factors, horizontal, and vertical shears, etc.). Factors such as the inherent device noise and error, the wind slip on the drifter, and behavior of the underlying Eulerian flow field contribute to the level of correlation. Spydell *et al*. [7] showed that drifter-Lagrangian and fixed device velocities are in good agreement in a tidal inlet ($R^2 > 0.92$), except at an ebb-tidal shoal where the velocity magnitude was low. With recent attention on drifter application in small tidal channels, there is a need for comprehensive assessments of what drifters are measuring within semibounded channels with preference in flow direction with moderate tidal currents. The current work provides an extensive evaluation of the Lagrangian drifter performance at a bounded inner section of an estuary with depth (2–3 m) and velocity scales (<0.5 m/s) supplementing [7] in a tidal inlet with depth up to 10 m (deep channel) and peak velocity >1 m/s.

Following the removal of selective availability, the accuracy of the GPS has improved, resulting in development of various small and robust drifters for near-shore and surf-zone applications [8], [10], [11]. The small spatial [O(1 m)] and short temporal [O(10 s)] scales of interest for mixing processes in estuaries require centimeter accuracy with high-frequency [O(1 Hz)] data acquisition. Thus in [12], a high-resolution (HR) drifter is described, with position accuracy ~1 cm, capable of sampling high frequency, and suitable in the absence of wave rectification for environments such as sheltered tidal estuaries and lakes with shallow depth as low as 0.5 m. A similar design equipped with an off-the-shelf GPS data logger is a low-resolution (LR) drifter, which designed for low-frequency measurements and position accuracy of between 2–3 m. Fig. 1 shows the spaghetti plots of drifter tracks from several deployments of clusters of these drifters (HR and LR) in a section of a shallow tidal estuary. The clustered tracks are used to examine surface turbulence properties and mixing through relative dispersion analyses and are discussed in greater detail elsewhere [4]. The aim here is to address the following questions regarding the drifter measurements, in addition to interpreting the observed flow field in a tidal channel.

1) What is the agreement between the drifter and fixed instrument velocity measurements in channel when in close proximity and what scale of fluctuation dictates such agreement?
2) What is the response of the drifter to wind and water currents within a tidal shallow estuary with moderate tidal current (<0.5 m/s)?
3) How does the wind affect the drifter motion?

Manuscript received November 19, 2017; revised April 17, 2018 and May 24, 2018; accepted June 17, 2018. Date of publication July 27, 2018; date of current version October 11, 2019. This work was supported in part by the Australian Research Council under the ARC Linkage Grant LP150101172 and in part by the Sunshine Coast Council. *(Corresponding author: Kabir A. Suara.)*

Associate Editor: M. Haller.

K. A. Suara and R. J. Brown are with the Science and Engineering Faculty, Queensland University of Technology, Brisbane, QLD 4000, Australia (e-mail: k.suara@qut.edu.au; richard.brown@qut.edu.au).

H. Wang, H. Chanson, and B. Gibbes are with the School of Civil Engineering, University of Queensland, Brisbane, QLD 4072, Australia (e-mail: hang.wang@uqconnect.edu.au; h.chanson@uq.edu.au; b.gibbes@uq.edu.au).

Digital Object Identifier 10.1109/JOE.2018.2850538

0364-9059 © 2018 IEEE. Personal use is permitted, but republication/redistribution requires IEEE permission.
See http://www.ieee.org/publications_standards/publications/rights/index.html for more information.

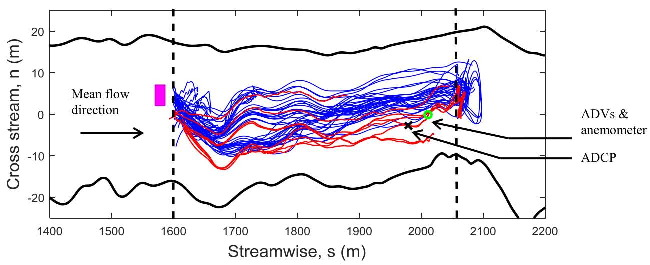

Fig. 1. Spaghetti plot of drifter tracks for LR drifter (blue tracks) and HR drifters (red tracks) EJ15E1 during a flood tide. The purple box indicates approximate drifters release zone, while the green "o" denotes ADVs (two units colocated with sampling volume vertically above each other) and wind ANE location. The black "*x*" indicates ADCP location. The solid black line represents the channel boundary.

II. Methods and Materials

A. Field and Experiment Descriptions

New observations of tidal flows from fixed and moving devices were collected in Eprapah Creek (Longitude 153.30° E, Latitude 27.567° S). The dynamics of the channel have been studied in the past, so as to understand turbulent mixing in a typical shallow estuary [13]. Eprapah Creek discharges into Moreton Bay on the east coast of Australia and consists of both straight and meandering sections. The estuarine zone extends up to 3.8-km inland and is well-sheltered from wind by adjacent mangrove vegetation communities. The field experiment was carried out for 48 h (July 29–31, 2015) along the relatively straight channel, downstream of site 2 (see Fig. 2). Drifter deployments were conducted during flood and slack tides within the straight test section between adopted middle thread distance (AMTD) 1.60–2.05 km, i.e., between cross sections B and D (see Fig. 2). Due to limited width and directional preference of the flow, a local coordinate, which moves with the flow, was chosen. Herein, "s" is the streamwise direction positive toward the channel mouth, whereas "*n*" is the cross-stream direction positive toward the left bank, and "u" is positive in upward direction.

A survey of bathymetry of the cross sections of the channel was conducted during the field study. The channel exhibits irregular boundaries, which may cause a high degree of variability in the cross-stream flow at different cross sections (see Fig. 2). Fig. 2 shows a map of the field sites and the cross sections close to the experimental test section. The maximum depth along the test section was about 2.5 m below the mean sea level. The channel width was about 60 m at high tide and 25 m at low tide.

B. Instrumentation

Descriptions of the instruments are summarized in Table I. Two acoustic Doppler velocimeters (ADVs) sampled continuously at 50 Hz. One ADCP, sampled continuously at 1 Hz, was placed approximately at the center of the channel 32-m downstream from the cross section where the ADVs were deployed. A 2-D sonic anemometer (ANE), sampled at a frequency of 4 Hz, was deployed to obtain the wind velocity near the water surface. The sample volume of ANE was placed about 1-m horizontal distance from ADV1 and 0.5 m above the free surface at the highest tide.

The HR drifters followed the design of [12] and were equipped with differential real-time kinematic (RTK) GPS integrated receivers and sampled at 10 Hz with position accuracy ∼2 cm. The LR drifters contained off-the-shelf Holux GPS data loggers with absolute position accuracy, between 2–3 m and were sampled at 1 Hz.

The drifters were positively buoyant for continuous satellite position fixation with <3 cm height unsubmerged to minimize the direct wind effect. The configuration results in a wind slip, estimated as less than 1% of the ambient wind, and is not accounted for in this analysis [12]. The drifters were deployed in clusters of 4 and 5 for three separate experiments. To evaluate the wind effects on the drifter motion and dispersion in the channel, two experiments were carried out during the flood tides with different wind intensities, whereas the third was carried out during a high slack water (see Table I). Note that the drifter deployments are identified by experiment, deployment, and resolution. For example E1 is experiment 1, D1 is deployment 1, and HR is high resolution. For each deployment, clusters were formed into polygons spaced ∼1 m between drifters while a time window of ∼3 min was maintained between cluster deployments. This creates a unique initial time and position for each deployment. The flood deployments were made at AMTD 1.6 km and collected at the end of the test section before redeployment from same initial point (see Fig. 2). The slack water deployments, on the other hand, were made within 100 m of the ADV.

C. Quality Control and Data Analysis

The ADV data sets were first postprocessed by removal of communication errors, data with correlation less than 60% and signal-to noise ratio less than 5 dB [14]. The upward looking ADCP data points, located in air and depth sidelobe effects (5% height from the surface), were removed using the water height measurements. Spikes resulting from external disturbances on the ADV and ADCP data sets are identified. The data sets were de-spiked using the phase-spaced thresholding technique (PST) [15]. Flagged data replacement here is aimed to ensure continuous data with respect to time, which is the prerequisite for the spectra and coherence analyses. Flagged and removed ADV data, which were less than 5% of the data set, were replaced using sample-and-hold technique, i.e., using previous valid data point [15], [16]. After removing measurements in air and those affected by surface reflection of the sidelobe in the ADCP, the spurious data points, identified by the PST, were generally less than 0.2% within the individual bin. These were replaced with linearly interpolated data at valid end points.

The drifter data sets were quality controlled by removal of data points and sections of the tracks where they were evidently trapped in the channel banks, obstructed or interrupted, based on the experimental event log. Spurious position data were identified as those with velocity and acceleration greater than some specified thresholds. The choice of the threshold is subject to the nature of the flow. The maximum tidal flow velocity in Eprapah Creek was about 0.3 m/s, thus a velocity threshold is defined as twice this velocity and an acceleration threshold of 1.5 m/s^2 in accordance with previous studies [17]. Flagged data were then replaced with linearly interpolated points using data at two valid end points if the gap was less than 20 s. Gaps greater than 20 s were considered omitted and were not replaced. The drifter data were transformed to channel-based streamwise (s), cross stream (n), and up (u) coordinate system following the work in [18] and [12]. For the HR drifters, the position time series was further treated with a lowpass filter of cutoff frequency, $F_c = 1$ Hz and subsampled to an interval of 1 s to remove the instrument noise at high frequency [12]. The velocities were obtained by central differencing of the quality controlled position time series. The position time series of the LR drifter contained some large uncertainty at frequencies greater than 0.01 Hz, which impaired the direction estimates, particularly during low flow speed. Therefore, to estimate the "true" (average) flow direction, the LR drifter position time series were lowpass filtered with $F_c = 0.01$ Hz obtained from

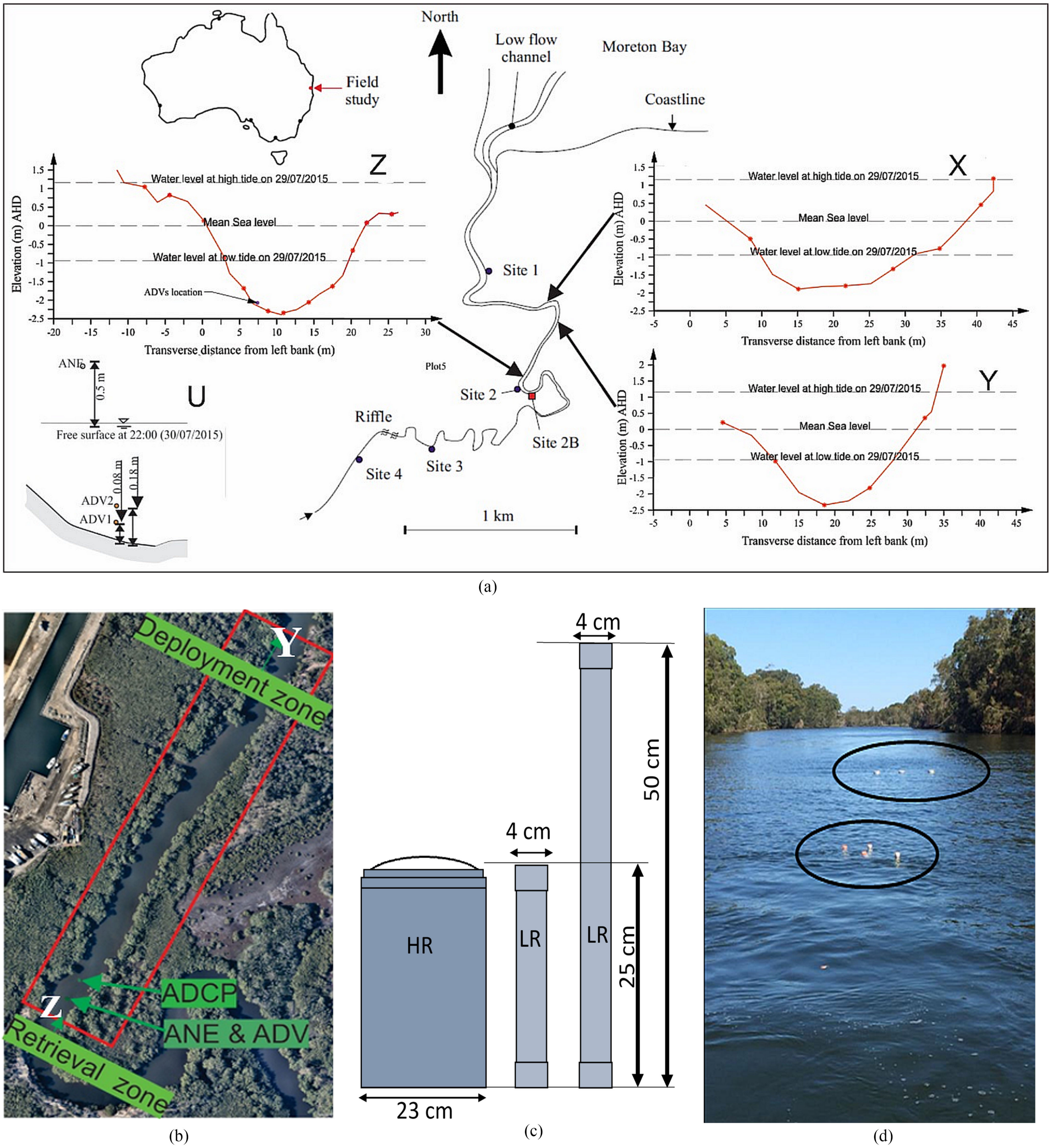

Fig. 2. (a) Eprapah Creek estuarine zone, including surveyed cross sections (X–Z) on July 30, 2015; drifter deployments were made at cross section (Y) while ADVs, and Sonic ANE were deployed downstream cross section (Z); U shows the instruments arrangement at ADV location. (b) Aerial view of Eprapah Creek (153.2931° E, −27.575° S) showing the experimental test section in red rectangle (Nearmap, 2015). (c) Dimensioned sketch of the LR and HR drifters. (d) Photograph of clusters of HR and LR drifters (black ellipse) about 2 min after deployment; upstream of cross section Y.

the method described in [12]. The velocities were then obtained by combining lowpass filtered position time series with the speed time series, S_p such that

$$V_S(t) = S_p(t) \times \sin\theta(t), \quad V_n(t) = S_p(t) \times \cos\theta(t)$$
$$\text{and} \quad \theta(t) = \arctan\left(\frac{s(t)}{n(t)}\right) \tag{1}$$

where V_s and V_n are the streamwise and cross-stream velocities, respectively, whereas θ is the direction based on the position time series (*s*, *n*).

D. Environmental Conditions

A range of tide, wind and flow conditions were encountered during the 48-h field study (see Fig. 3 and Table II). The average tidal

TABLE I
SAMPLING LOCATION AND INSTRUMENT DESCRIPTIONS

Instrument code (1)	Instrument description (2)	Sample / sensor head location (3)	Samp. Freq. (4)
ADV1	Sontek 3D-sidelooking microADV A813F (16MHz)	0.08 m above the bed 7.4 m from the left bank	50 Hz
ADV2	Sontek 2D-sidelooking microADV A641F (16MHz)	0.18 m above the bed 7.4 m from the left bank	50 Hz
ADCP	Nortek AquaDopp Profiler P27759 upward looking	0.1 m above the bed centre of channel at transect 32 downstream ADV1 location, Bin size = 10 cm	1Hz
HR	High resolution GPS-tracked drifters Cylinder with diameter, ϕ = 19 cm; height, h = 26 cm (~23 cm submerged)	Floating with pseudo-Lagrangian motion	10 Hz
LR	Low resolution Holux-GPS-tracked drifters Cylinder with diameter = 4 cm; height = 25 cm (22 cm submerged) & 50 cm (~43 cm submerged)	Floating with pseudo-Lagrangian motion	1 Hz
ANE	Sonic 2D anemometer	0.5 m above water level at high tide July 30, 2015	4 Hz

TABLE II
OVERVIEW OF THE ENVIRONMENTAL CONDITIONS OF THE FIELD DURING EXPERIMENT[a]

Experiment	Tidal type	Start time (s)	End time (s)	Tidal range (m)	Wind speed (m/s)	Average wind speed (m/s)	Wind Dir.(deg.)	Ave. surface V_H (m/s)
1	Flood	103,502	114,540	1.75	0 – 1.76	0.31	137	0.48
2	Flood	141,242	153,900	2.25	0 – 4.43	0.65	10	0.57
3	Slack	200,042	205,620	1.70	0 – 3.05	0.59	70	0.19

[a]Wind data from ANE with direction measured clockwise from positive streamwise direction downstream. Water surface horizontal velocity magnitude, V_H measured from the ADCP as average of the two valid upper bins after quality control. Time taken in (s) from 00:00 on July 29, 2015.

range was 2.03 m. Eprapah Creek is characterized with a diurnal wind pattern. The channel was reasonably sheltered, and the average wind between 0–4 m/s was mostly aligned with the streamwise direction during the day, and the night wind speed varied between 0–1 m/s without a directional preferee.

III. ANALYSES AND RESULTS

A. Temporal Variability of Velocity During the Field Studies

The major driving forces for circulation in an estuary can be categorized into wind and water currents. Before analyzing the response of the drifters to these forces, we present the temporal variability of the flow velocity next to the surface and the bed of the channel. Fig. 4 shows the time series of the mean horizontal flow velocity, $\bar{V}_{H}=\sqrt{\bar{V}_s^2+\bar{V}_n^2}$, for the ADCP bins next to the free surface, and the HR and LR drifters. The horizontal resultant mean velocities were obtained as moving averages with window size 200 s every 10 s along the individual data sets. The selections for the moving average are consistent with previous analysis of turbulent velocities at Eprapah Creek [19]. The surface flow showed a discernible tidal signal with the flood peak velocity $V_H \sim 0.5$ m/s greater than that of the ebb. Consistent with an open channel flow, the ADVs horizontal mean velocities next to the bed had magnitude significantly lower than those next to the free surface (see Fig. 5). The larger flood peaks were the result of the smaller cross-sectional area during the flood peak flows compared with the ebb flow. Slow fluctuations with periods between 1000 and 5000 s related to distance between landmarks/boundary structures were also captured in

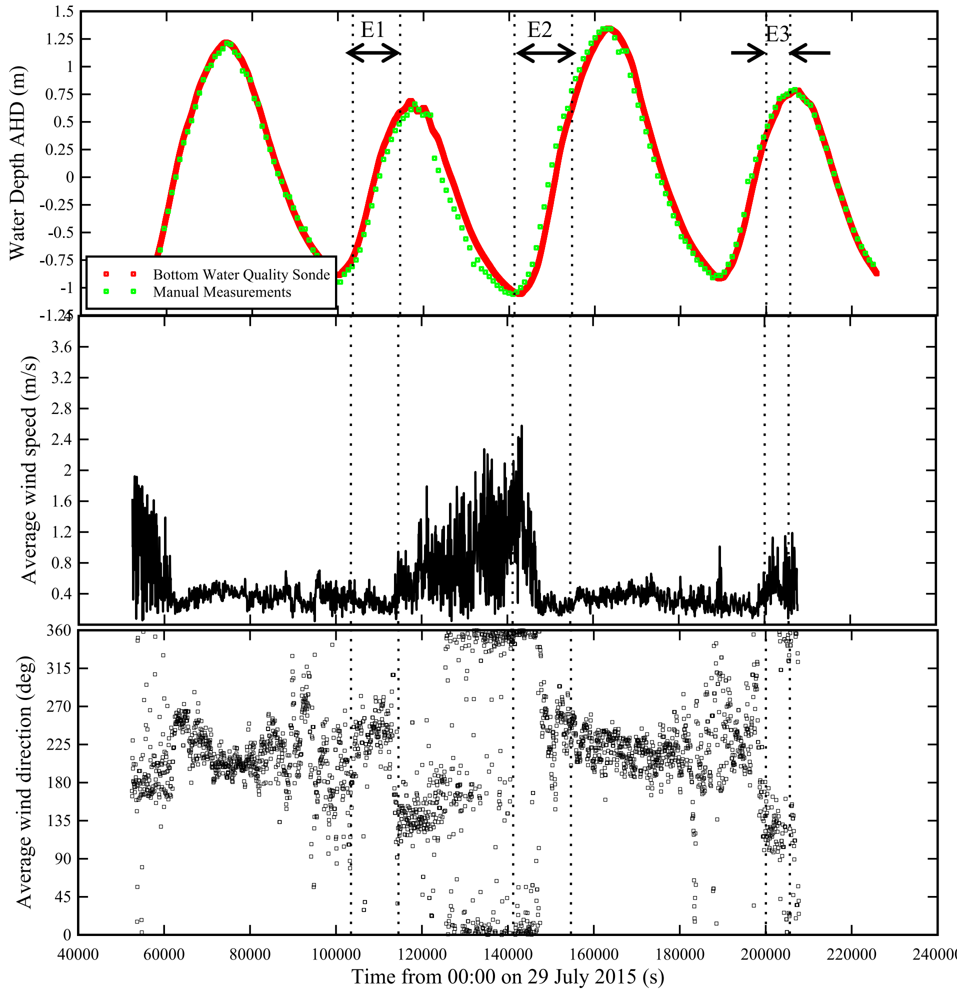

Fig. 3. Environmental conditions measured during the field work: (a) water level; (b) 1-min average wind speed; and (c) 1-min average wind direction clockwise from positive downstream direction. Water elevation collected in every 10 min at the ADV location and continuous measurement from a fixed probe. Wind data collected between 1–2 m above the water surface at the ADV location.

TABLE III
SUMMARY CORRELATION ANALYSIS OF THE DRIFTER-LAGRANGIAN AND FIXED-DEVICE-EULERIAN VELOCITIES[a]

Direction	Regression	ADCP-surface bins		ADCP Depth averaged		ADV(z = 0.18 m)	
		HR	LR	HR	LR	HR	LR
Streamwise	R^2	0.90	0.90	0.75	0.8	0.32	0.30
	RSME (m/s)	0.04	0.05	0.07	0.07	0.10	0.12
	I	1.00	1.10	0.91	1.0	0.91	1.20
Cross stream	R^2	0.02	0.02	0.1	0.1	0.09	0.03
	RSME (m/s)	0.016	0.013	0.016	0.01	0.017	0.014
	I	0.06	0.05	0.1	0.07	0.045	0.03

[a] R^2, RMSE, and I are, respectively, the correlation squared (R-squared statistic), standard deviation and the slope of a regression line between drifters (HR and LR) and fixed device (ADCP and ADV).

the velocity time series and spectral analyses. The slow fluctuation was observed throughout the period of observation and was strongest at slack water (e.g., 118 000–125 000 s). The presence of high-frequency fluctuations, "true" turbulence, was noticeable in the instantaneous velocity time series of the ADV and HR drifters. However, the LR and ADCP were dominated by noise at frequencies $F > 0.01$ Hz. Analyses of these fluctuations observed with the ADV and drifters, and their contributions to the mixing in the channel are presented elsewhere [17].

The drifter data obtained during the three experiments covered from 400-m downstream to about 100-m upstream of the fixed instruments, with their full time series of the mean horizontal velocities are presented in Figs. 4 and 5. The tidal and slow fluctuation signals were well captured by the ADCP, ADV, and drifters. The power spectral density (PSD) of the ADCP instantaneous velocities contained white noise at frequencies greater than 0.01 Hz, which overshadowed the turbulence measurements thus, higher frequency fluctuations could not be inferred

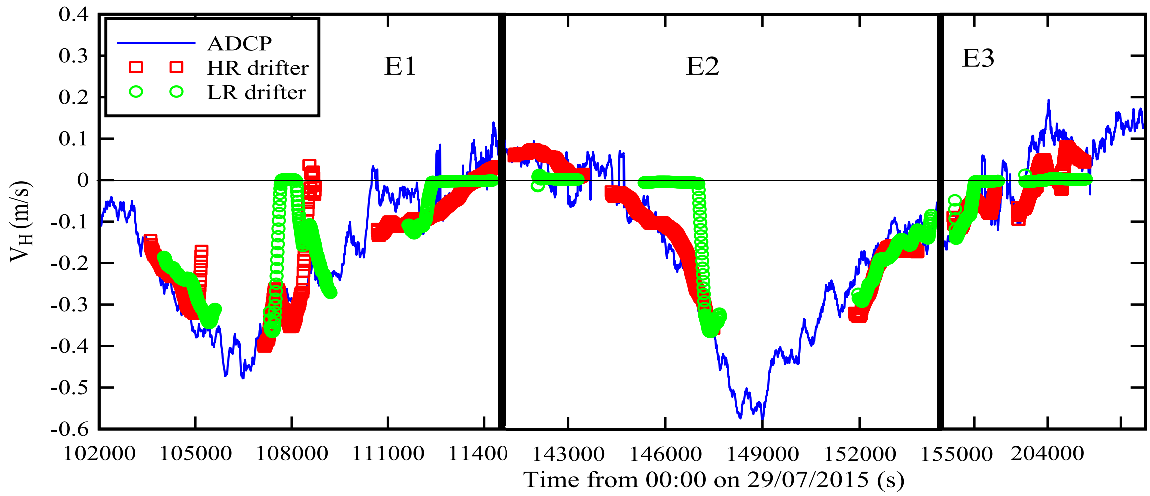

Fig. 4. Mean horizontal velocity for the surface measurements as a function of time for the ADCP, HR and LR drifters. Mean estimated by a moving average with window size 200 s every 10 s along individual data set. ADCP data are an average of the two last valid bins (20 cm) after correcting for depth variation and removing 5% depth sidelobe effects. The ADCP measurement depth compares with the submerged height of the HR drifter (23 cm): Positive direction during ebb tide—the thick vertical lines demarcate the window for different experiments.

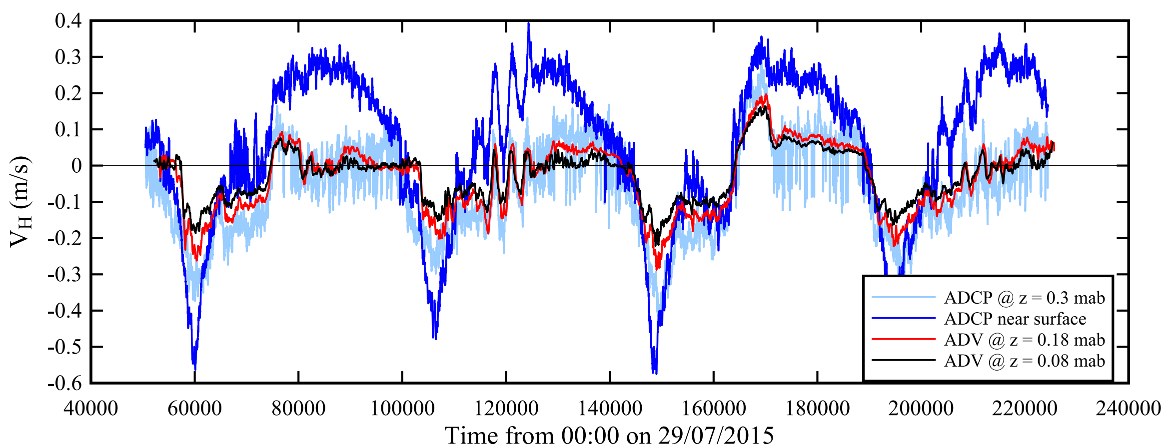

Fig. 5. Mean horizontal velocity as a function for surface measurements of the ADCP, ADCP lowest bin, and ADV measurements next to the bed. Mean estimated by moving average with window size 200 s every 10 s along individual data set.

from the ADCP. However, the time averaged velocity V_H for both HR and LR drifters was in good agreement with the ADCP surface measurements. While the velocities of the ADCP bin #1 at 0.3 mab were in good agreement with those of the ADV as expected, the magnitude of the ADV velocity was consistently smaller than that of the surface velocity. This reflected the locations of the ADV sampling volume at 0.08 and 0.15 m above the bed (see Table I and Fig. 2), where effects of boundary friction were significant.

B. Correlation Analysis: Lagrangian and Eulerian Measurements

The field study was designed such that clustered drifters passed through the cross sections where the fixed ADV and ADCP were installed. This provided a unique opportunity to directly compare the drifter-Lagrangian velocity with the fixed device-Eulerian velocity. Here, we analyze the response of the drifter to the underlying flow forces by identifying the extent of correlations that exist between the Lagrangian and Eulerian measurements. For each drifter deployment, the drifter-mean Lagrangian velocity, V_L at a fixed device is an average of velocity data point from all drifters that passed within a radius r of the fixed device following methods applied in [7]. However, because the flow field within the tidal channel changes rapidly with time, multiple drifter velocities from a single drifter passing through a fixed device can only contribute to V_L provided the instant is at most Δt from the time the first data point entered the virtual bin. To reduce the bias due to dependence of the residence time of drifters in a bin on the phase of the tide in the statistics, bins with degrees of freedom (DOFs) less than 5 are omitted in the comparisons. Here, the DOF is defined as

$$\mathrm{DOF}_{\mathrm{bin}} = \frac{\sum_{j=1}^{N} T_j^T}{T_L} \tag{2}$$

where T^T is the total time a single drifter spends in a bin, and N is the number of the drifter sampled within a bin, and $T_L \sim 20$ s is the Lagrangian integral time from ensemble autocorrelation function [20]. The corresponding Eulerian velocity V_E is the time averaged velocity of a fixed device between times corresponding to the first and last drifter

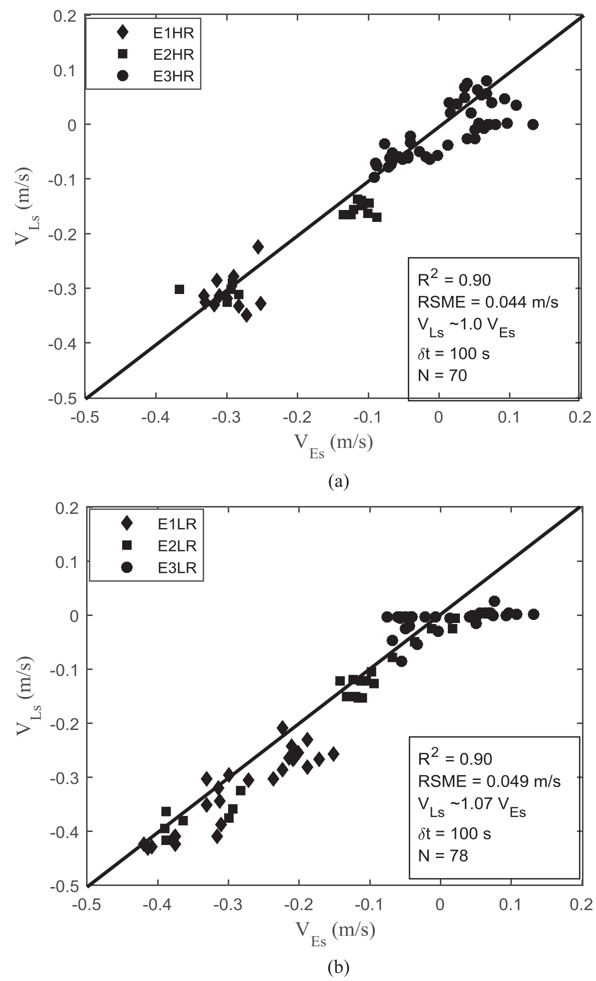

Fig. 6. Drifter-mean Lagrangian streamwise velocities (ADCP) versus mean Eulerian velocities for: (a) HR drifters; and (b) LR drifters. Each data point has a DOF ≥ 5.

velocities within the bin

$$V_E = \frac{1}{t_2 - t_1} \int_{t1}^{t2} V_i \delta t \tag{3}$$

where V_i is the instantaneous velocity from a fixed device and t_1, t_2 are the times of the first and last data points contributing to the corresponding V_L. With the ADCP surface measurements, sensitivity analysis was used to obtain values $r = 60$ m and $\Delta t = 100$ s. These choices were made as the smallest values combination that achieved the statistical stability (DOF ≥ 5) with most number of independent points. The correlation squared (*R*-squared statistic) R^2 and residual mean square error RMSE did not change appreciably with $r = 80$ m. Reducing *r* to 40 m reduced the number of points that fulfilled the constraint of DOF ≥ 5 to 40 without a significant change in the linear regression results. Similarly, the results were not affected with $\Delta t = 50$ and 200 s while $\Delta t < 50$ s introduced large scatter into the results and $\Delta t > 200$ s provided only 42 valid points. Table III summarizes the results of the correlation analysis between the Lagrangian and Eulerian measurements using the LR and HR drifters in turn against each of the ADCP surface flow velocity and ADV2 next to the bed.

Fig. 6 shows the comparison between the drifters and ADCP streamwise velocities for the three experiments. The ADCP surface velocities were depth average of two valid bins next to the free surface. Using all the data points from the three experiments (8-clustered deployments), the gradient of line of best fit was close to 1. The square correlation $R^2 = 0.90$ and RSME $= 0.04$ m/s between the drifter-Lagrangian streamwise velocity were obtained by forcing a zero intercept. The values of V_{LS} for experiment 2 were slightly underestimated using the drifter. This could be due to the upwind effect on the exposed portion of the drifters because the wind was predominantly streamwise positive during this period (see Fig. 2). Similar correlation ($R^2 = 0.9$, RSME $= 0.05$ m/s) was obtained between the LR drifters and the ADCP surface streamwise velocity (see Fig. 6). For both HR and LR drifters, the streamwise velocities were higher than the depth-averaged ADCP velocity and had lower correlation ($R^2 \sim 0.8$). An exception to the good agreement for the LR drifter was during slack water, experiment 3, where the water flow velocity magnitude was less than 0.1 m/s, which is the magnitude of inherent error in the speed estimate of the off-the-shelf GPS data-logger as specified by the manufacturer. With the exception of experiment 2, V_L values were distributed on either side of the regression lines. On the other hand, there was no significant correlation ($R^2 < 0.1$) between the drifter-Lagrangian and the ADCP surface-Eulerian cross-stream velocities. This might be linked to the strong variability in the cross-stream flow direction and low magnitude of the cross-stream velocity ($|\mathrm{V_n}| < 0.05$ m/s). The drifters and the ADV velocities near the bed were not significantly correlated ($R^2 < 0.35$ streamwise, $R^2 < 0.1$ cross stream). The instruments captured different scales of motion due to their difference in location and the sampling volumes.

In summary, the data showed that the drifters' observations have strong correlation in streamwise velocities with the surface and depth-averaged ADCP velocities, and lower correlation with the ADVs next to the bed within a horizontal radius $r = 60$ m of the fixed instrument. However, the correlation of cross-stream velocities of the drifters with the fixed instruments was low. This procedure assumed that the instruments sampled the same flow field, whereas tidal shallow water flows are highly spatially variable with small integral time scales (O [10 s]) and limited width. In a similar validation procedure in a surf-zone, Schmidt *et al*. [8] found very good agreement in streamwise direction, while the cross-stream correlation was low, attributed to the difference in location of the instruments. Similarly despite the good overall agreement ($R^2 > 0.92$) between the Eulerian–Lagrangian comparisons in a tidal inlet, the ebb shoal had low correlation [7]. This highlights the difficulty in a direct Eulerian–Lagrangian comparison in a bounded flow with a nonuniform boundary.

C. Velocity Spectra of Drifter, ADCP, and ADV

Here, we examine the spectra of the velocities obtained using the Eulerian and Lagrangian devices. Fig. 7 shows the PSDs of the ADV1 and ADCP surface flow during the 48-h observation period in the streamwise and cross-stream directions. The two sampling volumes were 32 m apart horizontally and 1.1–3.3 m vertically, due to change in water level. The streamwise velocity spectra highlights discernible peaks at the low frequency, for example, $F = 0.000025$ Hz, and $F = 0.0004$–0.0001 Hz likely associated with the tidal signal and the slow fluctuations, respectively. The streamwise and cross-stream spectra show that the noise floor of the ADCP was significant at a high frequency. Because of the high noise level of the ADCP at the frequency range ($F > 0.01$ Hz), where the drifter observations were made, the drifter velocity spectra were compared with those of the ADV1 only.

Fig. 8 shows sample PSD of streamwise and cross-stream velocities obtained concurrently from the ADV and HR drifters during the slack water experiment 3. This period is chosen because the mean flow effect was the least, allowing for a reasonable comparison of the Eulerian and

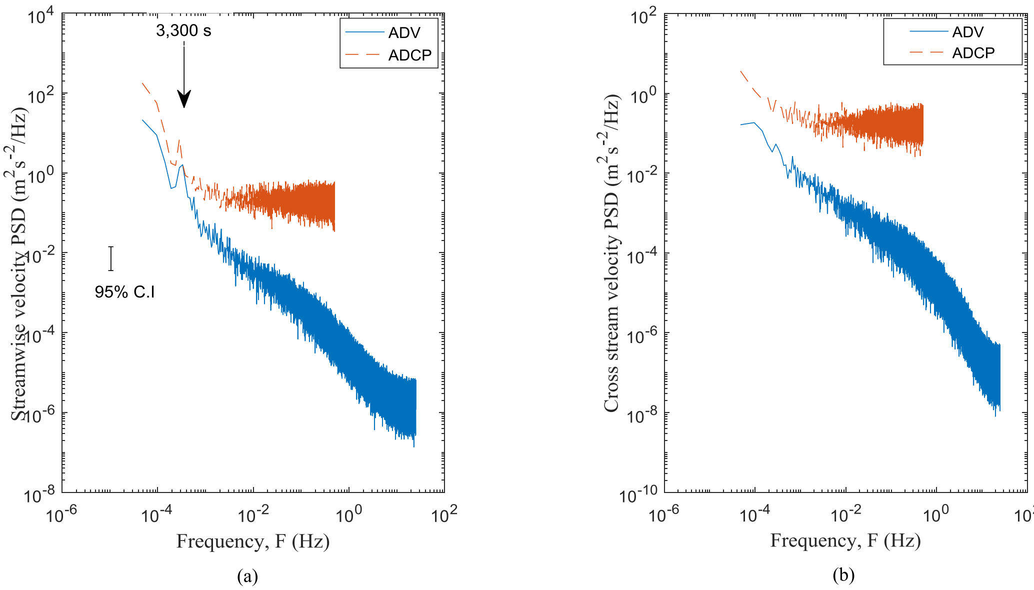

Fig. 7. ADV and ADCP surface flow velocity spectra during the 48-h field study. (a) Streamwise direction. (b) Cross-stream direction. The spectra are pwelch average estimate of five sections from the entire data set, windowed with a Hamming window and 50% overlap, resulting in at least 10 DOF.

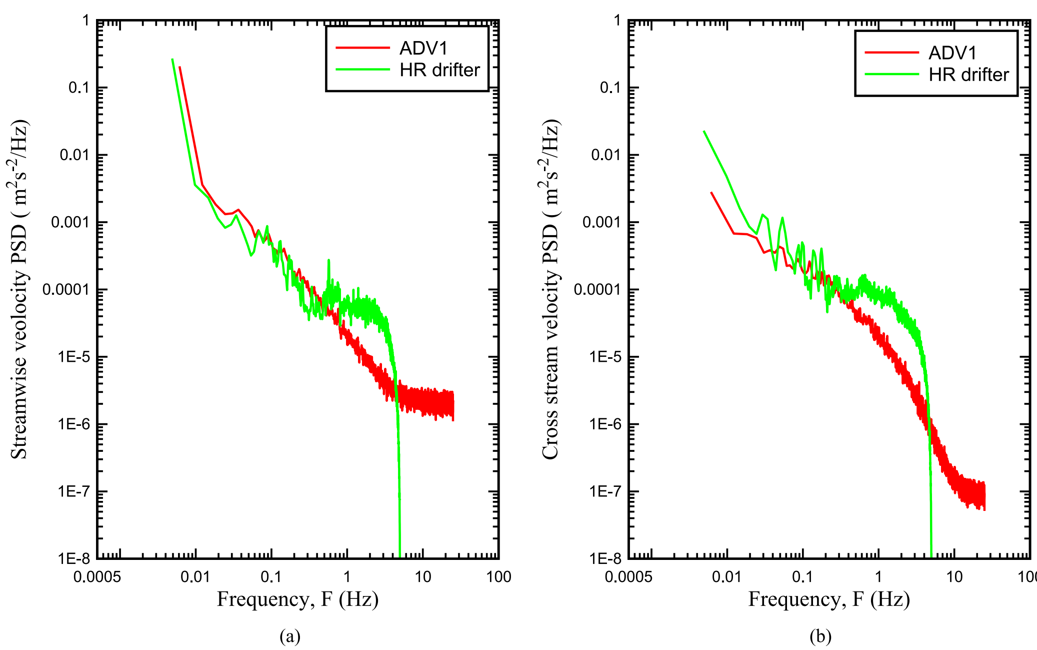

Fig. 8. HR drifters and ADV (49 min) velocity spectra during experiment 3. The drifters were within 60 m of the ADV. (a) Streamwise direction. (b) Cross-stream direction. The spectra are pwelch average estimate of five sections from the entire data set windowed with a Hamming window and 50% overlap, resulting in at least 10 DOF.

Lagrangian spectra. During this period, the drifters were within 60-m horizontal radius of the ADV1 and the vertical separation was between 2.4–2.7 m. To observe the spectral level of the HR drifters at a high frequency, the velocity sampled at 10 Hz were used in the analysis. The PSD for the HR drifters and ADV1 were similar in shape and magnitude within frequency $F = 0.001$–0.5 Hz in both flow directions. In [21] and [22], the buoyant and natural rolling frequencies, based on the geometry of the HR drifter, were estimated as $\sim$1 Hz. Therefore, the trough in PSD of the drifter velocity at about 0.8 Hz was related to the bobbing and rocking of the drifter hull in response to surface waves, while the rolloff in the velocity spectra at $F > 3$ Hz was associated with the filtering effect of the central differencing scheme used in estimating the velocity from the position time series. The similarity in shape and magnitude between the ADV1 and drifter velocity spectra shows that both instruments sampled the similar flow field at frequency < 0.5 Hz.

D. Coherence Analysis: Lagrangian and Eulerian Measurements

In this section, coherence analysis is used to examine the linear relationships, if any, between the drifters and driving forces by assuming that the measurements from fixed devices are an accurate measure of the local flow fields. Coherence is a measure of the extent of relationship between two time series as a function of frequency. Assuming a linear input–output relationship between a forcing factor *x* and response factor *y* in the frequency domain, the mean square coherence (MSC) is the normalized square cross spectrum between the spectra of *x* and *y* such that [23]

$$\mathrm{MSC}(F) = \frac{|P_{xy}(F)|^2}{P_{xx}(F).P_{yy}(F)} \tag{4}$$

where $P_{xx}(F)$ and $P_{yy}(F)$ are the power auto spectra of *x* and *y*, respectively, whereas $P_{xy}(F)$ is the complex cross spectrum between *x* and *y*, and *F* is the frequency. Magnitude of MSC varies between 0 and 1, indicating the incoherent and coherent values for an infinite length time series, respectively. With the assumption of linearity of the system, factors that can reduce the magnitude of MSC include noise or uncorrelated turbulence, as well as variance from other forcing input parameters. Because of the finite length of the time series within the radius *r* that the Lagrangian drifters could be assumed to resolve the same flow field as the Eulerian device, an independent threshold (IT) is defined such that

$$\mathrm{IT} = 1 - \alpha^{\left(\frac{1}{N_d - 1}\right)} \tag{5}$$

where α is the confidence interval, herein 0.95 and N_d is the number of independent cross spectral realizations in each frequency band [24]. To reduce the noise level in the MSC estimate for meaningful interpretation, a reasonably large value of N_d is required and N_d within 10–20 is suggested [25]. For consistency of interpretation and to reduce noise in MSC estimate, herein $N_d = 20$, equivalent to IT $= 0.15$ at 95% confidence interval is used irrespective of the varying length of the time series. This value ensures that frequency $F = 0.01$ Hz, equivalent to $\Delta t = 100$ employed in the correlation analysis is included in the coherence analysis for the shortest realization. The results were similar for all the HR drifter outputs except for difference in effective length. However, for consistency, the results of a single drifter with significantly long time series across the different analysis are presented throughout this section. The coherence between input and output signals is considered significant for MSC > IT, while coherence is insignificant for MSC in the neighborhood of or below IT.

1) Coherence Between Wind and Drifters: In drifter applications, quantifying the effect of the wind on the motion of the drifter is important to understand the actual water flow induced transport. Although only 3-cm height of the drifters was unsubmerged, direct wind drag is inevitable. The wind slip has been estimated using empirical models and force balance to be less than 1% of the ambient wind [12]. Another mechanism of wind that could influence drifter motion is the wind-induced water flow. Herein, the input time series are the wind velocities measured at about 1-m above the water surface, and the output time series are the velocities of an HR drifter within 60 m of a sonic ANE.

Fig. 9 shows the MSC estimates between the wind and the drifter velocity components. For experiments 1 and 3, the MSC values for both directions were below IT $= 0.15$ because of low wind energy during the experiments (see Fig. 3). The MSC values are greater than IT at a low frequency ($F < 0.04$ Hz) in the streamwise direction, except for slack water experiment 3, where the surface flow had no dominant direction. Similarly, for experiments 1 and 2 the MSC values were above the IT at a frequency around 0.3 Hz in the streamwise direction. This occurs around the frequency of wind-induced surface wave. Using longer drifter time series, the phase estimate in the streamwise direction indicated that the low-frequency wind ($F < 0.01$ Hz) was in phase with the drifter motion, while the drifter motion lagged the wind between 0.01–0.3 Hz (not shown). The estimates of the MSC in the cross-stream directions were not significant, except during the flood experiment 2, where an MSC ~ 0.3 was attainted at some frequencies with the wind signal leading the drifter at these frequencies [see Fig. 9(b)]. This coherence observation suggested that drifter motion at low and high frequencies is influenced by the local wind to some degree.

To understand the main mechanism responsible for wind influence on drifter motion in a sheltered estuary, coherence analyses with wind time series as an input and surface flow measured by the ADCP as an output was employed. In addition, analysis between the water surface velocities and the drifter was carried out using the portion of the data set corresponding to the times where the wind influence was most pronounced [see Fig. 9(b), experiment 2]. Fig. 10 shows that there was no significant difference between the level of coherence of the wind on the surface streamwise velocities measured by the HR drifter and the ADCP particularly at low frequencies ($F < 0.02$ Hz). Consequently, the coherence level between the drifter and ADCP measured streamwise velocities was higher than 90% (i.e., MSC > 0.9) at these low frequencies. The coherence level at higher frequency similarly increased suggesting that the instruments captured the same flow field, which was masked by differences in instrumental noise floor observed from the velocity spectra. The wind, drifter, and surface bin velocities were all in phase at low frequency with phase angle close to zero. It can therefore be deduced that the drifter responded more to the wind-induced surface flow velocities than the direct wind drag on the unsubmerged portion of the drifter. The magnitudes of MSC for the cross-stream velocities between the wind and the surface ADCP bin data were greater than those of wind against the drifter velocities. However, the values were not significantly higher than the 0.15 across the observed frequency to make a meaningful comparison.

2) Coherence Between the ADCP (Surface Flow), ADV, and Drifters: As shown in Fig. 10, the MSC between the drifter and ADCP surface flow was higher than IT at low frequency $F < 0.05$ Hz, while higher frequency estimate of MSC was corrupted by ADCP measurement noise floor. At low frequencies, the ADCP velocities lagged those of the drifter for experiment 1, while there was no phase difference between these instruments for experiments 2 and 3 in the streamwise direction. The cross-stream MSC values were not significantly above IT at all frequencies due to the strong variability of the channel cross sectional flow. This result was consistent with the lack of linear correlation in the velocities measured by the two instruments.

Fig. 11 shows the MSC between the velocities measured by ADV next to the bed and the drifter. The results show that the MSC values at low frequency ($F < 0.05$ Hz) were significantly greater than 0.15 in the streamwise direction for all the experiments. During the slack water experiment 3, the coherence between the drifters and the ADV (see Fig. 9) at low frequency is better than the corresponding coherence between the drifter and ADCP (see Fig. 11). This is likely due to the noise level of the ADCP, which is higher when compared with other instruments, and not significantly lower than the variance of the flow at this period. The MSC values in the cross-stream direction were predominantly lower than the IT, with the exception of experiment 2, where drifter velocities showed some level of coherence with the ADV velocities at high frequency ($F > 0.05$ Hz) in both the streamwise and cross-stream directions. This suggests that the instruments sampled the same flow field, while the low magnitude of MSC on the other hand suggests that the instruments captured different sizes of eddy and different parts of the flow field. For example, the drifter sampled surface flow, while the ADV sampled the flow field next to the bed. Therefore at an instance of time, the instruments sampled different part of eddies moving past the sampling location.

Coherence analysis results obtained using the LR drifters' velocities as output against the wind, ADCP and ADV velocities input were similar to those for the HR drifter at low frequencies ($F < 0.02$ Hz),

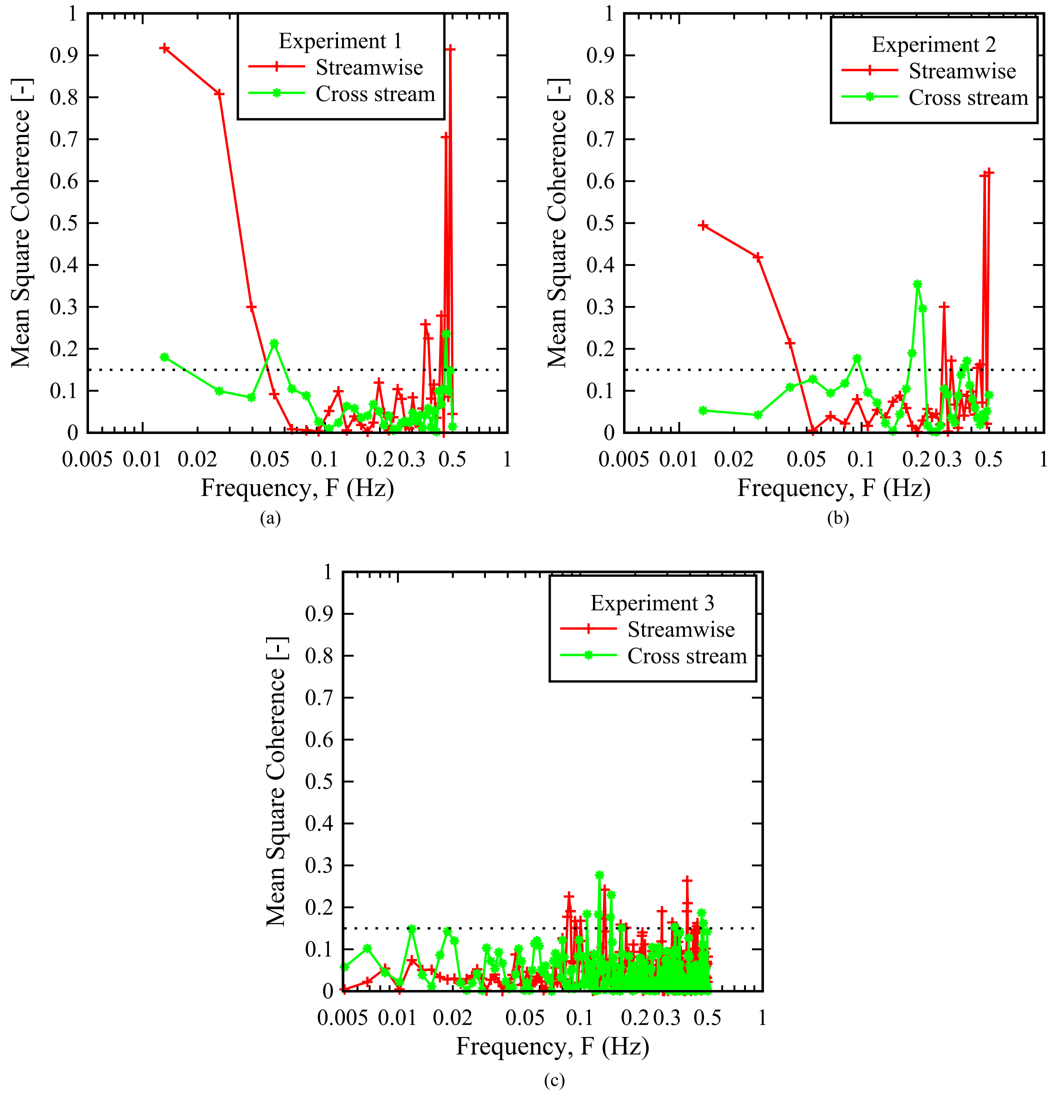

Fig. 9. Coherence between near water surface wind velocity and the HR drifter measurements for: (a) experiment 1; (b) experiment 2; and (c) experiment 3. Dashed horizontal line indicates the estimated incoherence level for bivariate white noise with DOF, DOF = 20 at 95% confidence interval. Note that the logarithmic scale on x-axis clusters the noisy MSC values at higher frequency.

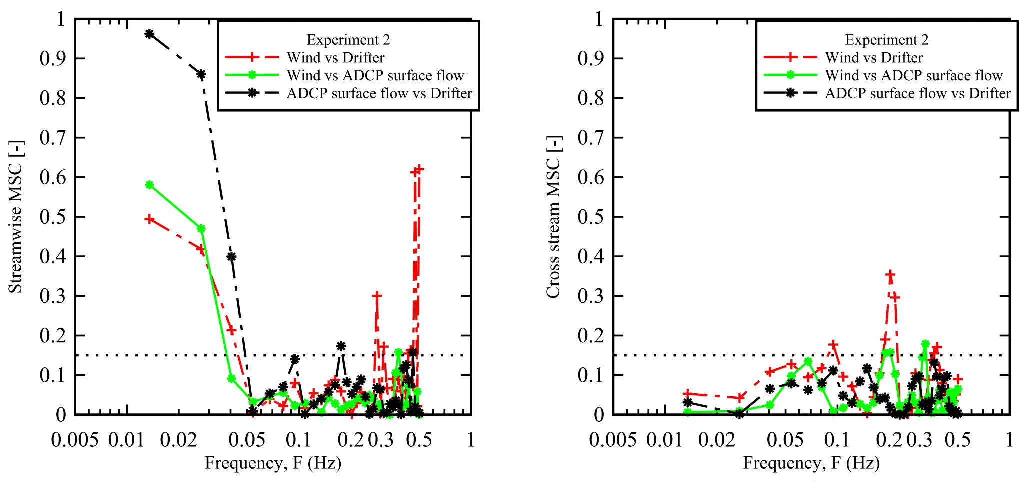

Fig. 10. Coherence between near water surface wind velocity, surface ADCP and the HR drifter measurements during experiment 2. (a) Streamwise direction. (b) Cross-stream direction. Dashed horizontal line indicates the estimated incoherence level for bivariate white noise with DOFs, DOF = 20 at 95% confidence interval.

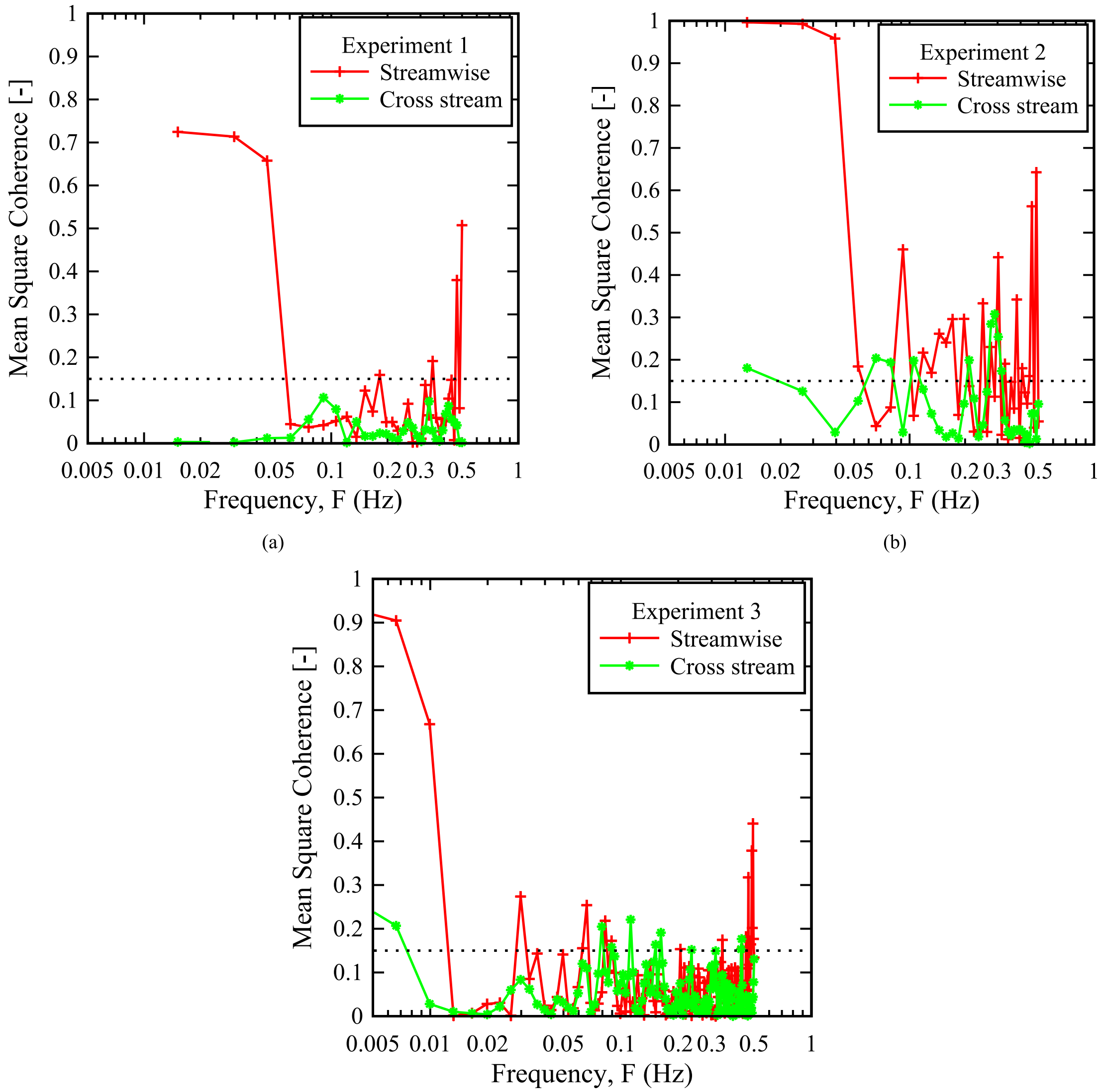

(a) (b) (c)

Fig. 11. Coherence between ADV velocities and the HR drifter measurements for difference experiments. (a) Experiment 1. (b) Experiment 2. (c) Experiment 3. Dashed horizontal line indicates the estimated incoherence level for bivariate white noise with DOFs, DOF = 20 at 95% confidence interval.

where the signal to noise ratios were higher than 10 (not shown). This suggested that both HR and LR drifters captured similar low-frequency ($F < 0.01$ Hz) velocity fluctuations next to the free surface of the channel.

E. Low/High Correlation and Coherence Between Eulerian and Lagrangian Data

Considerable research is presented in the literature on approaches to estimating Eulerian statistics (such as spectra, integral scales, and advection times) of a flow field from the Lagrangian observation and vice versa [26]–[28]. Analyses have shown that such Eulerian–Lagrangian transformations are dependent on the integral times and length scales of the underlying Eulerian flow field [26], [29]. Therefore, the observations obtained from Eulerian and Lagrangian frames of reference in a turbulent flow field are fundamentally different. Similarly, in an idealized isotropic stationary turbulent flow, two instruments separated by distances significantly larger than the eddy length scale are expected to have zero coherence because they are sampled independently. The associated turbulence field in a tidal channel contain eddies consisting of a wide range of sizes. This, coupled with the rapid change in flow direction in the cross-stream direction due to limited width, suggested that the Eulerian flow field in the channel had strong spatial variation.

The time scales of the velocity time series used in this analysis are estimated through velocity autocorrelation functions following [20]. The Lagrangian time scales from the drifter velocities T_L were approximately 20 and 15 s in the streamwise and cross-stream directions, respectively. The decorrelation time scale from the concurrently sampled ADV velocities T_{ADV} for all the experiments were less than half of those obtained from the drifter velocities, suggesting that the drifters captured larger scale eddies compared with the ADV. Thus, the sampling volume of the instrument acts as a lowpass filter that limits the sizes of the eddy sampled, while noise level impaired the coherence of the drifter with the fixed instruments, particularly the ADCP at high frequency. This further explains that the observed low level of coherence—observed at frequencies where noise levels were not significant—as well as the low correlation between the Eulerian and

Lagrangian devices is likely due to results of the instruments capturing different parts of the flow field. The high level of coherence at low frequency indicates that the bulk of drifter streamwise motion is directly related to the tidal and wind-forced surface flow.

IV. Discussion

There are many apparent difficulties associated with the use of drifters in shallow tidal water, which include trapping in channel banks, signal interference from overhanging vegetation, and limited boundaries amongst others. Despite these, HR and LR drifters have proven to be robust and easy to deploy in tidal environments with high spatiotemporal flow variation. A field study was carried out by deployments of clusters of LR and HR drifters in tidal shallow water to assess the dynamics of the surface flow and response of the drifters to the relevant driving forces. The flow was significantly more energetic close to the water surface than near the bed. Peak velocities during the flood tides were larger than those of the ebb, which might be linked to some tidal pumping effect.

Validation of drifter measurements in tidal shallow water is important to assess the nature and characteristics of GPS-tracked drifter measurements. This requires direct comparison of drifter measurements with those of fixed Eulerian devices. The correlation of the drifter data within 60 m of a fixed ADCP showed good agreement with the surface bin measurements (square correlation, $R^2 > 0.9$) and the depth averaged velocities ($R^2 > 0.75$) in the streamwise direction. Low correlation ($R^2 \sim 0.1$) was observed in the cross-stream direction and in the comparison of the drifter velocities with the ADV measurements next to the bed.

Coherence analysis was used to assess the response of the GPS-tracked drifters to scales of motion responded to, by assuming a linear single input–output system. For wind velocity magnitudes between 0–4 m/s, the analysis showed a strong level of coherence between the drifter response and wind input at frequencies $F < 0.02$ Hz, suggesting some wind influence on the drifter. This high level of coherence was mainly attributed to the response of the drifters to the wind-induced water flow next to the free surface, particularly in the streamwise direction. The result also highlighted an increase in coherence level with the increased wind energy at higher frequencies.

The analysis of the drifter response to the Eulerian velocity inputs showed that the drifter captured similar flow fluctuations for frequencies, $F < 0.01$ Hz in the streamwise direction, consistent with the correlation analysis. The result suggested that all drifters captured low-frequency streamwise velocity fluctuations in the free surface of the channel. Such drifters are therefore applicable to studying the dynamics of similar water bodies in relation to processes in the order of O [100 s] and larger. The coherence and correlation between the Lagrangian and Eulerian velocities at higher frequencies and in the cross-stream flow were typically low for the observation. On the other hand, comparison of the ADV and HR drifter velocity spectra in the streamwise and cross stream directions suggested that both instruments sampled the same flow field at frequencies up to 1 Hz. In addition, the HR drifters were shown to capture higher frequency processes with eddy size limited to those in the range of drifter characteristic length, and accurate at frequency up to 1 Hz [12]. Therefore, the low magnitude correlation and coherence observed are likely associated with difference in the Lagrangian–Eulerian observations and size of the eddy captured by the instrument dictated by the sampling volume size.

V. Conclusion

The assessments and analyses of flow field data collected in a microtidal estuary have shown that HR and LR drifters designs are applicable to studying the flow dynamics of tidal water bodies in relation to processes in the order of O [100 s] and larger. Under moderate wind conditions (0–4 m/s), floating drifter motions in bounded sheltered water are affected by wind through low-frequency induced wind current when only a small portion of the drifter is unsubmerged. The field validation of both HR and LR drifters, with surface measured velocity from an ADCP, is good ($R^2 > 0.9$; RSME $= 0.04$ m/s) in the streamwise direction while that of the cross stream is low associated with the high spatiotemporal variability of the velocity field, separation of the instrument and the difference in sampling volumes. It is shown that the bulk of drifter motion is directly related to the tidal and wind-forced surface flow within a shallow estuary with low tidal flow velocity (<0.5 m/s). Drifters have potential as a valuable tool to augment Eulerian measurements in tidal shallow water investigation and management, including estimates of eddy diffusivities [20] and apparent diffusivities. As drifter application, shallow water estuaries are just recently receiving some attention, further refinements in design are recommended to increase the range of processes drifters can resolve. Refinement of shallow water drifter design could include reduction of drifter overall size without degrading the tracking accuracies and compromising the water following capability to capture smaller scale processes of interest to shallow water bodies.

Acknowledgment

The authors would like to thank QUT and UQ volunteer undergraduates, who participated in the field study and data analysis, as well as the Queensland Department of Natural Resources and Mines, Australia, for providing access to the SunPOZ network for reference station data used for RTK postprocessing of the high-resolution GPS-tracked drifter. The authors also acknowledge the contributions of Dr. C. Wang to the work in analysis of the postprocessing of the RTK-GPS data.

References

[1] H. Chanson, R. J. Brown, and M. Trevethan, “Turbulence measurements in a small subtropical estuary under king tide conditions,” *Environ. Fluid Mech.*, vol. 12, pp. 265–289, Jun. 2012.

[2] M. Brocchini *et al.*, “Comparison between the wintertime and summertime dynamics of the Misa River estuary,” *Mar. Geol.*, vol. 385, pp. 27–40, 2017.

[3] A. Riddle and R. Lewis, “Dispersion experiments in UK coastal waters,” *Estuarine, Coastal Shelf Sci.*, vol. 51, pp. 243–254, Aug. 2000.

[4] K. Suara, H. Chanson, M. Borgas, and R. J. Brown, “Relative dispersion of clustered drifters in a small micro-tidal estuary,” *Estuarine, Coastal Shelf Sci.*, vol. 194, pp. 1–15, 2017.

[5] R. S. Tseng, “On the dispersion and diffusion near estuaries and around Islands,” *Estuarine, Coastal Shelf Sci.*, vol. 54, pp. 89–100, Jan. 2002.

[6] K. A. Whilden, S. A. Socolofsky, K.-A. Chang, and J. L. Irish, “Using surface drifter observations to measure tidal vortices and relative diffusion at Aransas Pass, Texas,” *Environ. Fluid Mech.*, vol. 14, pp. 1147–1172, Oct. 2014.

[7] M. S. Spydell *et al.*, “Observed and modeled drifters at a tidal inlet,” *J. Geophys. Res., Oceans*, vol. 120, pp. 4825–4844, 2015.

[8] W. Schmidt, B. Woodward, K. Millikan, R. Guza, B. Raubenheimer, and S. Elgar, “A GPS-tracked surf zone drifter,” *J. Atmos. Ocean. Technol.*, vol. 20, pp. 1069–1075, Jul. 2003.

[9] D. Johnson and C. Pattiaratchi, “Application, modelling and validation of surfzone drifters,” *Coastal Eng.*, vol. 51, pp. 455–471, 2004.

[10] D. Johnson, R. Stocker, R. Head, J. Imberger, and C. Pattiaratchi, “A compact, low-cost GPS drifter for use in the oceanic nearshore zone, lakes, and estuaries,” *J. Atmos. Ocean. Technol.*, vol. 20, pp. 1880–1884, 2003.

[11] J. C. Ohlmann, P. F. White, A. L. Sybrandy, and P. P. Niiler, “GPS–cellular drifter technology for coastal ocean observing systems,” *J. Atmos. Ocean. Technol.*, vol. 22, pp. 1381–1388, Aug. 2005.

[12] K. A. Suara, C. Wang, Y. Feng, R. J. Brown, H. Chanson, and M. Borgas, "High resolution GNSS-tracked drifter for studying surface dispersion in shallow water," *J. Atmos. Ocean. Technol.*, vol. 32, pp. 579–590, Mar. 2015.

[13] H. Chanson, "Field observations in a small subtropical estuary during and after a rainstorm event," *Estuarine, Coastal Shelf Sci.*, vol. 80, pp. 114–120, Oct. 2008.

[14] R. J. Brown and H. Chanson, "Turbulence and suspended sediment measurements in an urban environment during the Brisbane River flood of January 2011," *J. Hydraul. Eng.*, vol. 139, pp. 244–253, Feb. 2013.

[15] D. G. Goring and V. I. Nikora, "Despiking acoustic Doppler velocimeter data," *J. Hydraul. Eng.*, vol. 128, pp. 117–126, Jan. 2002.

[16] M. Parsheh, F. Sotiropoulos, and F. Porté-Agel, "Estimation of power spectra of acoustic-Doppler velocimetry data contaminated with intermittent spikes," *J. Hydraul. Eng.*, vol. 136, pp. 368–378, 2010.

[17] K. A. Suara, R. J. Brown, and H. Chanson, "Turbulence and mixing in the environment: multi-device study in a sub-tropical estuary," Div. Civil Eng., Univ. Queensland, Brisbane, QLD, Australia, Report No. CH99/15, (ISBN 1742721389), 2015.

[18] C. J. Legleiter and P. C. Kyriakidis, "Forward and inverse transformations between Cartesian and channel-fitted coordinate systems for meandering rivers," *Math. Geol.*, vol. 38, pp. 927–958, Nov. 2006.

[19] M. Trevethan, H. Chanson, and R. J. Brown, "Turbulent measurements in a small subtropical estuary with semidiurnal tides," *J. Hydraul. Eng.*, vol. 134, pp. 1665–1670, Nov. 2008.

[20] K. A. Suara, R. J. Brown, and M. Borgas, "Eddy diffusivity: a single dispersion analysis of high resolution drifters in a tidal shallow estuary," *Environ. Fluid Mech.*, vol. 16, pp. 923–943, 2016.

[21] J. Austin and S. Atkinson, "The design and testing of small, low-cost GPS-tracked surface drifters," *Estuaries*, vol. 27, pp. 1026–1029, 2004.

[22] W. Wawrzyński and P. Krata, "On ship roll resonance frequency," *Ocean Eng*., vol. 126, pp. 92–114, 016.

[23] J. S. Bendat and A. G. Piersol, *Random Data: Analysis and Measurement Procedures*, vol. 729, 4th ed. Hoboken, NJ, USA: Wiley, 2011.

[24] R. E. Thomson and W. J. Emery, *Data Analysis Methods in Physical Oceanography*. Amsterdam, The Netherlands: Elsevier, 2014.

[25] R. O. Thompson, "Coherence significance levels," *J. Atmos. Sci.*, vol. 36, pp. 2020–2021, Oct. 1979.

[26] J. F. Middleton, "Drifter spectra and diffusivities," *J. Mar. Res.*, vol. 43, pp. 37–55, 1985.

[27] O. Søren and M. Jakob, "An experimental test of Corrsin's conjecture and some related ideas," *New J. Phys.*, vol. 7, 2005, Art. no. 142.

[28] J. LaCasce, "Estimating Eulerian energy spectra from drifters," *Fluids*, vol. 1, 2016, Art. no. 33.

[29] R. Davis, "Oceanic property transport, Lagrangian particle statistics, and their prediction," *J. Mar. Res.*, vol. 41, pp. 163–194, 1983.

Kabir A. Suara received the B.Tech. degree in mechanical engineering from the Ladoke Akintola University of Technology, Ogbomosho, Nigeria, in 2009, the M.S. degree in mechanical engineering from the King Fahd University of Petroleum and Mineral, Dhahran, Saudi Arabia, in 2013, and the Ph.D. degree in mechanical engineering from the Queensland University of Technology (QUT), Brisbane, QLD, Australia, in 2017.

He is currently a Postdoctoral Fellow with the Environmental Fluid Mechanics Research Group, QUT. His research interests include turbulence in internal and external flows, development and evaluation of environmental monitoring instruments, and turbulent mixing in estuaries. His current research interests include bridging the gap between observation and modeling of estuarine transport processes using advanced Lagrangian observation tools and numerical approach with an improved accuracy through Lagrangian data assimilation.

Hang Wang received the Ph.D. degree in hydraulic engineering from the University of Queensland, Brisbane, QLD, Australia, in 2014.

He has a three-year postdoctoral research experience in experimental fluid mechanics and water engineering. He is currently an Engineer with Jeremy Benn Pacific, Spring Hill, QLD, Australia. He is currently working in flood forecasting and modeling, and coastal and hydraulic modeling.

Dr. Wang is the winner of the 2014 Lorenz G. Straub Award (presented in 2016 by St. Anthony Falls Laboratory, University of Minnesota).

Hubert Chanson received the Ph.D. degree in civil engineering from the University of Canterbury, Christchurch, New Zealand, in 1988.

He is currently a Professor in Civil Engineering, Hydraulic Engineering and Environmental Fluid Mechanics at the University of Queensland, Brisbane, QLD, Australia. He has authored or coauthored more than 850 international refereed papers and several books, and his work has been cited more than 4500 times (WoS) to 15 000 times (Google Scholar) since 1990. His research interests include design of hydraulic structures, experimental investigations of two-phase flows, applied hydrodynamics, hydraulic engineering, water quality modeling, environmental fluid mechanics, estuarine processes and natural resources.

Dr. Chanson was ranked among the 150 most cited researchers in civil engineering in Shanghai's Global Ranking of Academics. In 2018, his h-index is 33 (WoS), 36 (Scopus), and 60 (Google Scholar).

Badin Gibbes received the Ph.D. degree in environmental engineering from the University of Queensland, Brisbane, QLD, Australia, in 2007.

He is currently an Environmental Engineer at the School of Civil Engineering, University of Queensland, with more than 20 years of experience in the water resources field, where he leads the Equatic Systems Research Group. This group works in collaboration with water management authorities and the engineering consulting industry to combine innovate environmental monitoring systems with sophisticated numerical models to improve water quality management outcomes. He is also actively involved in the University of Queensland's undergraduate and postgraduate teaching programs, where he lectures in the areas of hydrology, water resources modeling, and environmental management.

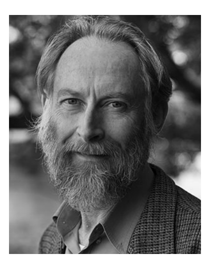

Richard J. Brown received the Ph.D. degree in mechanical engineering from the University of Sydney, Sydney, NSW, Australia, in 1996.

He is currently a Professor with the Science and Engineering Faculty, University of Queensland, Brisbane, QLD, Australia, the Director with the Biofuel Engine Research Facility, and the Leader with the Environmental Fluid Mechanics Group. He leads an active research groups consisting of postdocs, research fellows, early- mid-career academics and around half a dozen Ph.D. students. His environmental fluid mechanics research group collaborates with state and local councils on developing robust methods and schemes for managing estuarine and riverine systems from anthropogenic activities and natural pressures from boundary generated turbulence, tides, and coastal waves. His research interests include environmental fluid mechanics, emissions, pollution, smog formation, and applied thermodynamics.